From Eqs. (29) and (30), we find

$$f_{101}=\frac{eE_0}{m}\left(\frac{\omega\sin\beta z-\nu\cos\beta z}{\nu^2+\omega^2}\right)\frac{\partial f_{000}}{\partial v}, \quad (32)$$

and

$$g_{101}=\frac{eE_0}{m}\left(\frac{\nu\sin\beta z-\omega\cos\beta z}{\nu^2+\omega^2}\right)\frac{\partial f_{000}}{\partial v}. \quad (33)$$

To find the spherically symmetric $f_{000}$, we must solve

$$\frac{m}{M}\frac{\partial}{\partial v}(v^3\nu f_{000})+\frac{kT}{M}\frac{\partial}{\partial v}\left(v^2\nu\frac{\partial f_{000}}{\partial v}\right)+\left(\frac{eE_0}{m}\right)^2\frac{1}{6}\frac{\partial}{\partial v}\left(\frac{v^2\nu}{\nu^2+\omega^2}\frac{\partial f_{000}}{\partial v}\right)+\frac{v^4}{3\nu}\frac{\partial^2 f_{000}}{\partial z^2}=0. \quad (34)$$

Now because the force on the electrons is invariant to the transformation $z\rightarrow z+(2\pi/\beta)$, the distribution function must also be. Since $\beta$ does not appear in Eq. (34), it follows that if $f_{000}$ is invariant to the above transformation it must be independent of $z$. We are thus led to the familiar result[3]

$$\log f_{000}=-\int_0^{v^2}\frac{\frac{1}{2}md(v^2)}{kT+M(eE_0/m)^2/6(\nu^2+\omega^2)}+\text{const.} \quad (35)$$

Finally we use Eqs. (11a), (32), and (33) to obtain

$$j_x=-\frac{4\pi e^2E_0}{3}\left[\cos(\beta z-\omega t)\int_0^\infty\frac{\partial f_{000}}{\partial v}\frac{v^3\nu}{\nu^2+\omega^2}dv-\sin(\beta z-\omega t)\int_0^\infty\frac{\partial f_{000}}{\partial v}\frac{v^3\omega}{\nu^2+\omega^2}dv\right]. \quad (36)$$

Since $j_x=\mathrm{Re}\{\sigma_c E_0 e^{-i(\beta z-\omega t)}\}$, we obtain the familiar result given by Eq. (11b) for $\sigma_c$. We thus see that the conductivity is independent of position.


## ACKNOWLEDGMENTS

The author wishes to express his appreciation to Dr. T. E. Van Zandt for the use of his dissertation and to Professor Henry Margenau for many illuminating and encouraging discussions.


PHYSICAL REVIEW VOLUME 103, NUMBER 2 JULY 15, 1956

# Radiochemical Studies of the Interaction of Lead with Protons in the Energy Range 0.6 to 3.0 Bev*

R. WOLFGANG, E. W. BAKER, A. A. CARETTO,† J. B. CUMMING, G. FRIEDLANDER, AND J. HUDIS
*Chemistry Department, Brookhaven National Laboratory, Upton, New York*

(Received April 11, 1956)

Lead targets have been bombarded with protons of several energies between 0.6 and 3.0 Bev and formation cross sections have been determined for about 30 nuclides of $A<140$ produced in these bombardments. The excitation functions, both for the lightest products studied ($A<35$) and for neutron-deficient barium isotopes, rise steeply with increasing energy. For intermediate-mass products ($50<A<120$), the changes in formation cross sections with increasing energy are much smaller and may largely be interpreted as a shift towards more neutron-deficient products and as a broadening of the yield-mass distribution. At 3 Bev the spallation and fission product regions have merged, and the cross sections for forming all mass numbers below the target mass are equal within an order of magnitude. The changes in yield pattern above about 0.4 Bev are shown to be associated with increasing probabilities of very large energy transfers (of the order of 1 Bev) from the incident proton to the struck nucleus, and this trend is explained in terms of an energy transfer mechanism involving the production, scattering, and reabsorption of pions. Besides the well-known modes of de-excitation—particle evaporation (spallation) and fission—a new mode termed fragmentation is postulated to account for some of the observed products, especially the light fragments. Fragmentation is thought to be associated with the short mean free paths of pions in nuclear matter which cause local heating and can thus lead to dissociation of the nucleus into fragments in a time short compared to that required for equipartition of energy.

RADIOCHEMICAL studies of a wide variety of products resulting from the bombardment of bismuth with 340-Mev,[1] 480-Mev,[2] and 660-Mev[3] protons have been reported from other laboratories. At these energies the products fall quite distinctly into two mass regions, generally referred to as the spallation and fission regions, respectively. The so-called spallation products comprise nuclides within 30 or 40 units of $A$ of

* Research performed under the auspices of the U. S. Atomic Energy Commission.

† Now at Radiation Laboratory, University of California, Berkeley, California.

[1] W. F. Biller, University of California Radiation Laboratory Report UCRL-2067 (unpublished).

[2] Vinogradov, Alimarin, Baranov, Lavrukhina, Baranova, Pavlotskaya, Bragina, and Yakovlev, Conference of the Academy of Sciences, U.S.S.R., on Peaceful Uses of Atomic Energy, July 1–5, 1955; Session of Division of Chemical Sciences, p. 97 and p. 132. (English translation by Consultants Bureau, New York, U. S. Atomic Energy Commission Rept. TR-2435, Pt. 2, 1956, pp. 65 and 85.)

[3] Murin, Preobrazhensky, Yutlandov, and Yakimov, Conference of the Academy of Sciences, U.S.S.R., on Peaceful Uses of Atomic Energy, July 1–5, 1955; Session of Division of Chemical Sciences, p. 160. (English translation by Consultants Bureau, New York, U. S. Atomic Energy Commission Rept. TR-2435, Pt. 2, 1956, p. 101.)

the target, and their formation cross sections decrease sharply with decreasing $A$. The fission region, separated from the spallation products by a region of very low yields, extends from about $A=140$ downward, with a single peak in the yield-*vs*-mass curve centered at about $A=95$ for $E_p=340$ Mev and at about $A=90$ for $E_p=660$ Mev.[3] The radiochemical investigations quoted[1–3] indicate that fission accounts for approximately 7 to 15% of the total inelastic cross section of bismuth for energies between 340 and 660 Mev; however, they give somewhat conflicting evidence as to the absolute values and the energy dependence of the fission cross sections. By a more reliable direct fission-counting method, the ratio of fission to inelastic cross section for bismuth was shown[4] to increase monotonically from 0.06 at 100 Mev to 0.13 at 340 Mev. More recent radiochemical data[5] are in good agreement with this result and indicate that the fission cross section continues to increase slowly to 450 Mev.

Preliminary work in this laboratory on the interactions of 2.2-Bev protons with lead[6] and bismuth[7] indicated that the distribution of radioactive products at the bombarding energy differs markedly from the distributions observed at the lower energies. The valley between the fission and spallation regions in the yield-*vs*-mass plot is completely absent. In fact, at 2.2 Bev, the largest formation cross sections appeared to occur in the rare-earth region. Recently, marked increases in yields (up to factors of 4) in the range of $A=130$ to $A=180$ have been reported[3] for increases in proton energy from 480 Mev to 660 Mev. When the proton energy is raised to 2.2 Bev, the formation cross sections for nuclides in this mass range are increased by about two orders of magnitude.[7]

In view of the qualitative differences in the yield distributions observed at 340- to 660-Mev and at 2.2-Bev proton energy, it seemed of interest to obtain more detailed information on the energy dependence of formation cross sections of a variety of products from the bombardment of lead or bismuth with protons in the Cosmotron range. Lead rather than bismuth was chosen as the target material because of easier availability of lead target foils. The present paper reports excitation functions for the production of about 30 nuclides of $A\leqslant 140$, formed in the interaction of lead with protons in the energy range 0.6 to 3.0 Bev.

## EXPERIMENTAL

Irradiations were carried out in the circulating beam of the Brookhaven Cosmotron. Two lead foils, each approximately 90 mg/cm$^2$ thick, and a 21-mg/cm$^2$ aluminum monitor foil were lined up to superimpose precisely in a standard target holder. This target, with the aluminum monitor on the upstream side was inserted into the vacuum chamber from the inside of the accelerator doughnut. Because protons are lost out of the circulating beam during the acceleration cycle, it is necessary to protect the target from these low-energy particles. The usual method is to keep the target in a shielded position except at the end of each acceleration cycle, when a pneumatic ram propels it to an exposed position.[8] With this system, however, the lead foils used in the present experiments were found to tear after a few minutes. Therefore a different scheme was devised in which the target was in the bombardment position throughout the run, but was protected from low-energy contamination by a thick block of aluminum, 270° upstream from the target and radially one inch closer to the proton orbit. Near the end of the cycle this shadowing or "shutter" target was withdrawn by a pneumatic plunger, leaving the lead foils exposed to the full-energy beam as its orbit contracted after the end of rf acceleration. Bombardment energies were varied from 0.6 to 3.0 Bev by adjustment of the duration of rf acceleration. In general a one-hour bombardment gave adequate activity levels for the longest-lived products investigated.

After irradiation equal areas were cut out of the target foils. The $Na^{24}$ produced in the aluminum was determined by $\beta$ counting of the foil in a standard geometry, and the yield of the $Al^{27}(p,3pn)Na^{24}$ reaction was used as a measure of the beam intensity. The lead foils were dissolved in $6N$ $HNO_3$ containing 2–10 mg of each of the appropriate carriers. Usually no more than four elements were isolated from a given foil. The foil adjacent to the aluminum monitor foil was never used to measure the yields of products with $A<28$, because of the possible contribution of recoil fragments originating in the aluminum. The chemical separations carried out had to be capable of separating the desired element from all other known activities of atomic weight less than about 210. In general, adaptations of standard techniques were adequate for this purpose, but some new procedures were used and are described in the Appendix. The final precipitates mounted on small disks of filter paper were generally counted under end-window flow proportional counters of known geometry. In some cases these measurements were supplemented by $\gamma$ counting with scintillation counters and x-ray counting with a large gas-filled proportional counter and pulse-height analyzer. After the completion of decay measurements the samples were dissolved, and the chemical yield, that is the fraction of added carrier recovered, was determined for each sample by suitable analytical techniques.

Decay curves were analyzed into their components, and for each radioactive species the disintegration rate

[4] H. M. Steiner and J. A. Jungerman, Phys. Rev. **101**, 807 (1956).
[5] L. G. Jodra and N. Sugarman, Phys. Rev. **99**, 1470 (1955).
[6] J. M. Miller and G. Friedlander, Phys. Rev. **91**, 485 (1953).
[7] Sugarman, Duffield, Friedlander, and Miller, Phys. Rev. **95**, 1704 (1954).
[8] Friedlander, Miller, Wolfgang, Hudis, and Baker, Phys. Rev. **94**, 727 (1954).

TABLE I. Formation cross section (in millibarns) for products of the interaction of protons with lead.

| Product | Type of yield[a] | Proton energy (in Bev) 0.39 | 0.6 | 1.0 | 1.6 | 2.2 | 3.0 |
|---|---|---|---|---|---|---|---|
| $F^{18}$ | *C* | | 0.005[b] | 0.039 | 0.18 | 0.39 | 0.49 |
| $Na^{22}$ | *C* | | | | <2.2[b] | <1.5[b] | <2.7[b] |
| $Na^{24}$ | *C* | 0.03[b] | <0.02[b] | 0.36 | 1.4[b] | 2.3[b] | 3.6 |
| $Mg^{28}$ | *C* | ⩽0.001[b] | 0.024 | 0.075 | 0.27 | 0.48 | 0.59 |
| $P^{32}$ | *I* | ⩽0.01[b] | ~0.02[c] | 0.09 | 0.31 | 0.80 | 0.66 |
| $P^{33}$ | *C* | | | ~$10^{-2}$ [bc] | ~0.1[c] | ~0.2[c] | ~0.2[c] |
| $Ca^{45}$ | *C* | | | | <0.3 | | |
| $Ca^{47}$ | *C* | | <0.6[b] | | 0.076[b] | <0.1[b] | |
| $Mn^{56}$ | *C* | | | 1.3 | 1.3 | 1.1 | 1.3 |
| $Fe^{52}$ | *C* | | | <0.001[b] | <0.008[b] | | |
| $Fe^{59}$ | *C* | | ⩽0.5 | 0.5 | 0.64[b] | 0.81 | 0.70[b] |
| $Cu^{61}$ | *C* | | 0.07[bc] | 0.08[bc] | 0.09[c] | 0.22[c] | 0.21[bc] |
| $Cu^{64}$ | *I* | | 0.47[b] | 0.71 | 0.89 | 1.1 | 1.3[b] |
| $Cu^{67}$ | *C* | | 0.58[b] | 0.74 | 0.68 | 0.65 | 0.57[b] |
| $Zn^{62}$ | *C* | | | ⩽0.006[b] | ⩽0.006[b] | | ⩽0.01[b] |
| $Zn^{69m}$ | *C* | | 0.55[b] | 0.95 | 1.1 | 0.95 | 1.1[b] |
| $Zn^{71m}$ | *C* | | | 0.6[c] | 0.51[c] | 0.41[bc] | 1.0[bc] |
| $Zn^{72}$ | *C* | | 0.39[b] | 0.37 | 0.35 | 0.28 | 0.35[b] |
| $Ga^{66}$ | *C-I* | | ⩽0.01 | ⩽0.03 | | ⩽0.1 | |
| $Ga^{67}$ | *C-I* | 0.013[bc] | 0.43[c] | 0.24[c] | 0.56[bc] | 1.1[c] | |
| $Ga^{72}$ | *I* | 0.56[bc] | 1.06[bc] | 0.68[c] | 1.08[bc] | 0.89[c] | |
| $Ga^{73}$ | *C* | 1.2[b] | 1.3[b] | 0.57 | 0.83[b] | 0.81 | |
| $Mo^{93m}$ | *I* | | 0.14 | 0.31[b] | 0.44[b] | 0.78 | 0.63[b] |
| $Mo^{99}$ | *C* | | 3.5 | 2.6[b] | 1.9 | 1.6 | 1.1[b] |
| $Cd^{107}$ | *C-I* | | 0.13[c] | 0.5[bc] | 0.52[c] | 0.82[c] | 1.0[bc] |
| $Cd^{115}$ | *C* | | 0.32 | 0.25[b] | 0.16 | 0.14 | 0.11[b] |
| $Cd^{115m}$ | *I* | | 0.55 | 0.5[b] | 0.33 | 0.35 | ~0.24[b] |
| $Cd^{117m}$ | *C* | | 0.2[c] | | 0.1[bc] | 0.07[c] | 0.03[bc] |
| $Ba^{128}$ | *C* | | 0.20[b] | 0.46 | 2.1[b] | 5.4[b] | 6.0[b] |
| $Ba^{129}$ | *C* | | 0.062[b] | 0.32 | 2.5[b] | 5.8[b] | 6.0[b] |
| $Ba^{131}$ | *C-I* | | 0.11[b] | 0.96[b] | 2.5[b] | 6.1[b] | 7.7[b] |
| $Ba^{133m+135m}$ | *C-I*(?) | | <0.1[b] | <0.1[b] | <0.6[b] | <1.0[b] | <1.2[b] |
| $Ba^{140}$ | *C* | | ⩽0.05[b] | ⩽0.1[b] | ⩽0.2[b] | ⩽0.5[b] | ⩽0.5[b] |

[a] *C* denotes cumulative yield of mass chain beta-decaying to given nuclide; *I* denotes independent yield of given nuclide; *C-I* denotes cases intermediate between *C* and *I* (half-life of precursor comparable to the time required for separation).
[b] Value based on one run only.
[c] Estimated error greater than ±20%. See Appendix.

for infinitely long bombardment was computed by corrections for length of bombardment, chemical yield, counting geometry, and intrinsic counting efficiency. For emitters of hard $\beta$ rays the combined effects of window absorption, self-absorption, and self-scattering were found to be small enough to be neglected and back-scattering was assumed to be independent of $\beta$ energy. Those cases, in which absorption corrections were required and those in which the counting efficiency differed from unity, are discussed in the Appendix.

To convert saturation disintegration rates to absolute cross sections a knowledge of the proton beam intensity in each run was required, and this was calculated from the yield of the Al($p$,3$pn$)$Na^{24}$ reaction in the monitor foil. The excitation function for this reaction has been reported in an earlier paper.[9] It should be noted that all absolute cross section values in the present paper are subject to the ±30% limit of error assigned[9] to the monitor cross section. A correction was applied for the small amount of $Na^{24}$ produced in the monitor foil by secondary particles originating in the lead. In separate experiments the contribution of these secondaries to the $Na^{24}$ production was found to be about 5% at proton energies between 1 and 3 Bev; in these experiments the ratio of the Al($p$,3$pn$) reaction to a reaction insensitive to particles below ~0.6 Bev—the production of the $\alpha$-emitting $Tb^{149}$ from gold[10]—was measured with and without lead foils placed downstream from the monitors.

A few excitation functions were extended below 600 Mev by irradiations with 385-Mev protons in the Nevis cyclotron.

## RESULTS

The cross sections obtained are given in Table I and most of them are also depicted graphically in Figs. 1–6. About half the values given are averages based on two or more runs. Errors arise from a number of sources. Relative monitoring by means of the aluminum foils is probably accurate within a few percent. Errors arising from counting statistics and from uncertainties in absorption, self-absorption, and back scattering may amount to about 15%. Analysis of complex decay curves resulted in uncertainties of about 10% in the yields of the shorter-lived activities. The chemical yield determinations were generally accurate to 5%. Altogether it is believed that the uncertainty of the reported cross sections is about ±20%. Certain cases in which the estimated error is higher than 20% are indicated in

[9] Friedlander, Hudis, and Wolfgang, Phys. Rev. **99**, 263 (1955).

[10] Duffield, Friedlander, and Miller (to be published).

Table I and mentioned in the Appendix. This estimate of the errors in the individual cross sections is in addition to the previously mentioned systematic uncertainty in the absolute cross-section standard used.

The excitation functions shown in Figs. 1 to 6 exhibit trends which appear to be correlated with the mass numbers of the products. For the heaviest nuclides studied, the neutron-deficient barium isotopes, the cross sections rise steeply with increasing energy (Fig. 1). This is in accordance with the previous observation[6,7] that the valley between the fission and spallation regions fills in at Bev energies. At 340 to 660 Mev bombarding energies,[1–3,11] approximately 90% of the interactions lead to products of $A>180$. With 2.2-Bev protons the largest product yields occur[6,7] in the region $140<A<200$.

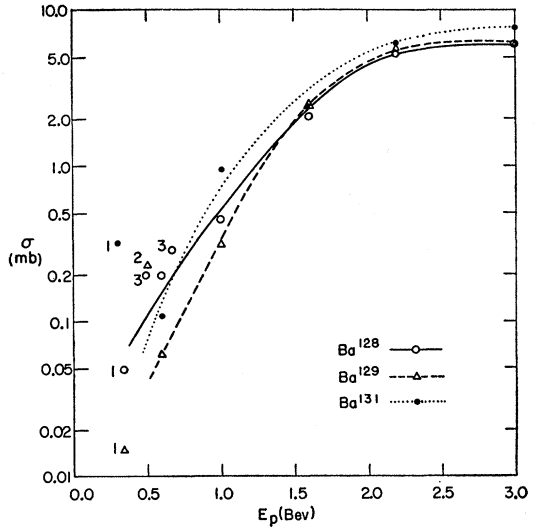


FIG. 1. Excitation functions for the production of neutron-deficient barium isotopes in proton bombardments of lead. The points in Figs. 1 through 6 labeled 1, 2, and 3 are from references 1, 2, and 3, respectively, and refer to bismuth, rather than lead targets.

The excitation functions for medium-mass products show quite a different behavior. The cross sections for producing the neutron-deficient nuclides observed ($Cu^{61}$, $Ga^{67}$, $Mo^{93m}$, $Cd^{107}$) increase by factors of 3 to 10 from 0.4 to 3 Bev (Fig. 2). On the other hand, the excitation functions of those neutron-excess nuclides which are produced in high yields by fission at the lower energies decrease with increasing energy (Fig. 3). Figures 4 and 5 show that cross sections for formation of neutron-excess products in the range $55<A<75$ remain fairly constant over the energy range studied; these are the nuclides which form the low-mass wing of the fission-yield curve at the lower energies.

The cross sections for producing the low-mass species ($P^{32}$, $Mg^{28}$, $Na^{24}$, $F^{18}$) exhibit the most interesting

[11] W. E. Bennett, Phys. Rev. **94**, 997 (1954).

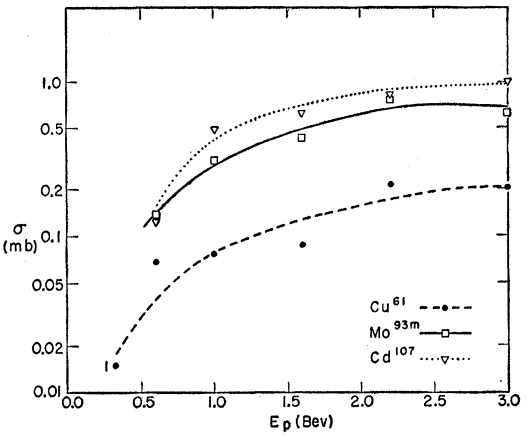


FIG. 2. Excitation functions for the production of some neutron-deficient nuclides in proton bombardments of lead.

behavior (Fig. 6). They rise very steeply with increasing energy up to about 2 Bev and then remain fairly constant.

Figure 7 gives a representation of the change in the over-all yield spectrum between 0.34 and 3 Bev. The data of Biller[1] on bismuth fission at 340 Mev, and those of Vinogradov *et al.*[2] on spallation and fission of bismuth at 480 Mev are compared with the 3-Bev lead data of the present paper. Experimental points are not shown; rather an attempt has been made to give an approximate representation of the total formation cross section per mass number as a function of $A$. The interpolations are certainly crude, and the true mass-yield distribution at 3 Bev may well exhibit details of structure not shown in the figure. Above $A\sim130$, other published[7] and unpublished data from this laboratory have been used to extend the 3-Bev curve. If there is a fission peak in the 3-Bev yield-mass curve, it certainly does not stand out very clearly. The absence of the deep valleys in the regions of $A\approx150$ and $A\approx50$ makes it difficult to attribute the formation of particular products to dif-

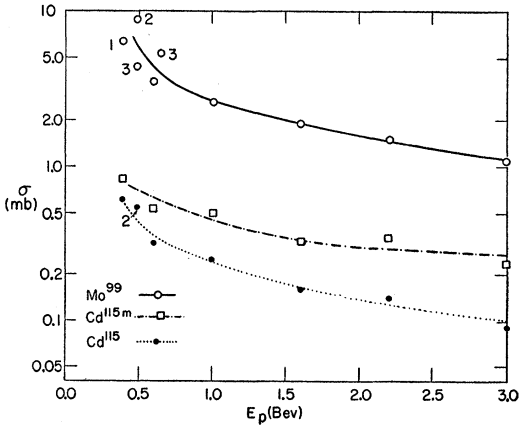


FIG. 3. Excitation functions for the production of some neutron-excess nuclides in proton bombardments of lead.

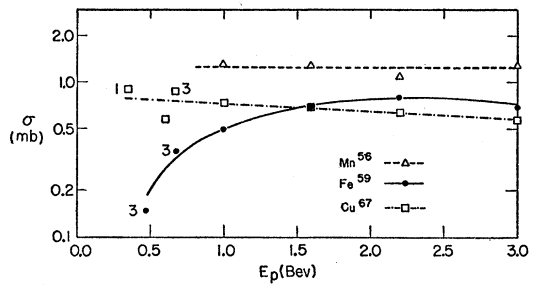


FIG. 4. Excitation functions for the production of some neutron-excess nuclides in proton bombardments of lead.

ferent and clearly distinguishable mechanisms. It is a rather remarkable result that, at 3 Bev, the cross section for forming any mass number below the target mass is the same within an order of magnitude.

The change in yield patterns between 0.6 and 3.0 Bev is shown even more clearly in Fig. 8. This plot of the ratio of cross sections at these two energies empahsizes the great increase in yield of the lighter products. In addition it shows the diverging trend between neutron-excess and neutron-deficient species above mass 70.

## DISCUSSION

The experimental results may be discussed in terms of mechanisms for the transfer of energy to the struck nuclei and subsequent dissipation of this energy leading to the observed products.

### Mesons as Vehicles for Energy Transfers

The observation[6,7] that nuclides in the range $120<A<180$, such as $Ba^{128,129}$ and $Tb^{149}$, are produced with cross sections of several millibarns in the bombardment of lead or bismuth with 2.2-Bev protons led to an investigation of their recoil properties.[7,12] The forward momenta of these product nuclei were found to be of such a magnitude as to require energy transfers of the order of 1 Bev from the incident proton to the struck nucleus. The barium excitation functions reported here

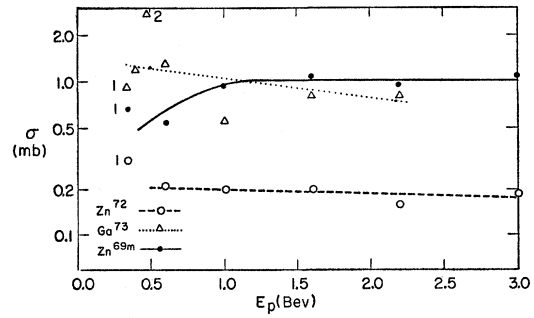


FIG. 5. Excitation functions for the production of some neutron-excess nuclides in proton bombardments of lead.

[12] Sugarman, Campos, and Wielgoz, Phys. Rev. **101**, 388 (1956).

(Fig. 1) may then be considered as reflecting a steep increase with bombarding energy in the probability of such large energy transfers. Simultaneously the probability of deposition of excitation energies in the 100-Mev range appears to decrease with increasing bombarding energy. This trend is indicated by the declining cross sections of neutron-excess fission products (Fig. 3). These nuclides are formed in high yield at a few hundred Mev bombarding energy and, even at 2.2 Bev, one of them, $Sr^{91}$, has been shown[12] by recoil studies to be produced in events in which only little energy is transferred. Such a shift in the energy deposition spectrum with incident energy has already been postulated[8] to account for the data of copper spallation with 2.2-Bev protons.

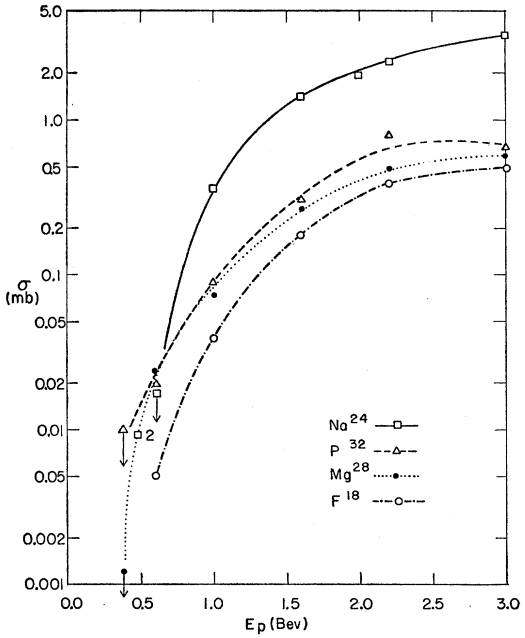


FIG. 6. Excitation functions for the production of light nuclei in proton bombardments of lead.

According to the simple nucleon-nucleon knock-on model as developed to account for energy transfers from incident particles of a few hundred Mev,[13–15] the amount of energy transferred increases only slowly as the energy of the projectile increases. However, above about 0.4 Bev creation of mesons in nucleon-nucleon collisions becomes significant, and it has been suggested[16] that meson processes become important agents for energy transfers to struck nuclei. This notion will now be elaborated.

The $\pi$ mesons created in nucleon-nucleon collisions

[13] R. Serber, Phys. Rev. **72**, 1114 (1947).
[14] M. L. Goldberger, Phys. Rev. **74**, 1269 (1948).
[15] Bernardini, Booth, and Lindenbaum, Phys. Rev. **85**, 826 (1952).
[16] R. L. Wolfgang and G. Friedlander, Phys. Rev. **96**, 190 (1954).

have been shown[17] to have energy spectra which are quite sharply peaked at low energies (at ~100 Mev in the center-of-mass system) and which shift only slightly with incident nucleon energy in the range of 1 to 3 Bev. Thus, most of the pions produced inside a nucleus by incident protons in the Bev range have energies in the region of the large resonance peak[18] in the pion-nucleon cross section and therefore have short mean free paths in nuclear matter. For example, for a $\pi^+$ meson of 200-Mev kinetic energy (near the peak of the resonance), the mean free path in a Pb nucleus is about one tenth the nuclear radius. The probability that a pion produced inside a heavy nucleus escapes without additional scattering collisions is thus negligibly small, and

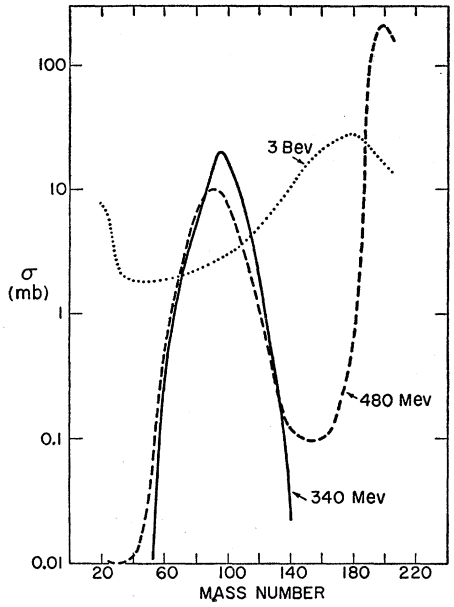


FIG. 7. Cross sections as a function of product mass number for the interaction of lead or bismuth with protons of various energies. An attempt has been made to represent total cross sections for each mass number. The 3-Bev curve is based on the data in the present paper up to $A \sim 130$, and on references 6 and 7 and unpublished bismuth data of R. B. Duffield for higher $A$. The 480-Mev curve (for bismuth) is taken from the data of Vinogradov *et al.* (reference 2), the 340-Mev curve (also bismuth) is reproduced from Biller (reference 1).

in most cases there will be several pion-nucleon scatterings. Because of the rather low kinetic energies of the pions, the energy transfer in any such scattering collision will be small (generally <50 Mev) so that the struck nucleons will usually not escape but contribute to nuclear excitation. In addition to the large scattering cross section, pions in nuclear matter will also have appreciable cross sections for absorption by pairs of nucleons, and for this process too there appears[19] to be

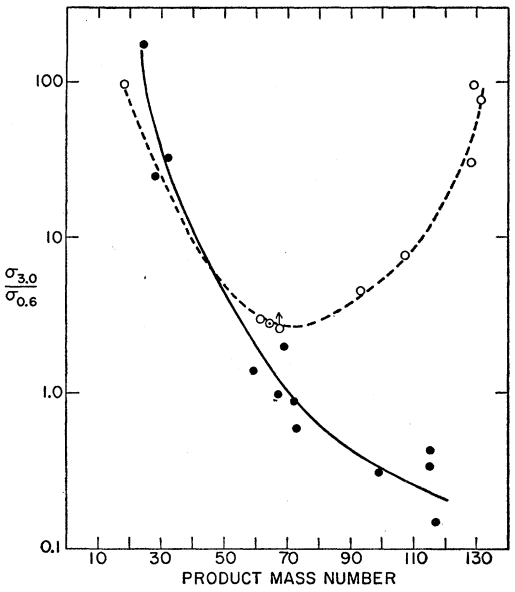


FIG. 8. Ratios of formation cross sections at 3.0 Bev to those at 0.6-Bev proton energy for various products. Solid circles represent neutron-excess nuclides, open circles neutron-deficient nuclides.

a resonance at a pion energy of ~140 Mev. There is then a reasonable probability that the total energy of a pion created inside a large nucleus (including its rest energy) is converted into nuclear excitation. These considerations have found fairly direct confirmation in emulsion work on the interaction of negative pions of 500-Mev kinetic energy with silver and bromine nuclei[20]; in these studies relatively few pions were seen to leave nuclei struck by incident pions.

Between 350 and 1000 Mev, the inelastic *pp* cross section increases from zero to 29 mb,[21,22] and the inelastic *pn* cross section also rises, although to a somewhat smaller value. This increase in pion production coupled with the pion scattering and reabsorption just discussed supplies a qualitatively satisfactory explanation for the rapidly rising excitation functions for processes requiring large excitation energies. The decrease in cross sections for reactions requiring smaller excitation is also accounted for. Above about 1 Bev the inelastic nucleon-nucleon cross sections vary only slowly. However, further increases in average energy transfers may still be expected because the multiplicity of pion production per inelastic collision increases[17,23] from one at 1 Bev to between two and three at 3 Bev. As already pointed out, the energy spectra of mesons produced are not strongly dependent on proton energy over this range, so that the energy transfer mechanisms

[17] L. C. L. Yuan and S. J. Lindenbaum, Phys. Rev. **93**, 1431 (1954), and private communication.
[18] S. J. Lindenbaum and L. C. L. Yuan, Phys. Rev. **100**, 306 (1955).
[19] M. G. Meshcheryakov and B. S. Neganov, Doklady Akad. Nauk U.S.S.R. **100**, 677 (1955).
[20] M. Blau and M. Caulton, Phys. Rev. **96**, 150 (1954); M. Blau (private communication).
[21] Shapiro, Leavitt, and Chen, Phys. Rev. **95**, 663 (1954); Chen, Leavitt, and Shapiro, Phys. Rev. **103**, 212 (1956).
[22] Smith, McReynolds, and Snow, Phys. Rev. **97**, 1186 (1955).
[23] Fowler, Shutt, Thorndike, and Whittemore, Phys. Rev. **95**, 1026 (1954).

discussed continue to apply. In addition to multiple pion production, plural production should also be of some importance at the highest proton energies.

Although meson processes provide a mechanism for the transfer to a target nucleus of very large excitation energies, it is clear that there will actually be a very broad spectrum of energy transfers extending all the way down to zero. Glancing collisions at the periphery of the nucleus will lead to small energy transfers at all bombarding energies; but with increasing bombarding energy above the meson production threshold and up to 2 or 3 Bev, the most probable value of energy deposition will shift to higher energies. Quantitative predictions of the energy deposition spectrum as a function of incident energy must await the results of a Monte Carlo calculation now being carried out by N. Metropolis, A. Turkevich, and J. M. Miller.

### Processes Following Energy-Transfer Cascade

The energy deposited in the nucleus may be dissipated in various ways. In this section the processes following the energy deposition cascade and leading to the final product distribution will be discussed in terms of three mechanisms: spallation, fission, and fragmentation. The first two of these are operative at lower bombarding energies also, the last is thought to be characteristic of the energy range above the meson production threshold and closely connected with the mesonic energy transfer mechanism discussed.

#### *1. Spallation*

Over the entire energy range studied, the formation of the most abundant products, those of $A > \sim 130$, is thought to result largely from a spallation mechanism, that is evaporation of nucleons and other small fragments from the excited nucleus remaining after the knock-on and energy-transfer cascade. The trend towards increasing average energy transfers with increasing bombarding energy is clearly reflected in the change in yield patterns of these spallation products with proton energy: the peak of the spallation yields shifts from $A \approx 200$ to $A \approx 180$ as the proton energy goes from 0.3 to 3 Bev (Fig. 7), and the formation cross sections of barium isotopes (Fig. 1) and rare earth nuclides[7] rise steeply with energy.

In other words, at 3-Bev bombarding energy, spallation events involving the evaporation of as many as 60 or 70 nucleons or their equivalent appear to be rather probable. However, as will be discussed below, products in the region of barium may not be *entirely* formed by spallation. Also as the excitation energy increases, the distinction between the knock-on and evaporation phases of a spallation reaction probably becomes rather fuzzy. At 1-Bev excitation, one presumably does not deal with a true evaporation mechanism in the sense that thermodynamic equilibrium is continually maintained. Rather, there is likely to be a smooth transition as far as both time scale and energies of emitted particles are concerned, from emission by pure knock-on to an evaporation mechanism. The lightest nuclides produced may well be evaporated particles and in that sense can be considered complementary to the spallation products. The yields of $H^3$,[24] $He^6$,[25] and $Be^7$ [26] from various target elements are probably consistent with this interpretation.

#### *2. Fission*

Most of the yields of products with mass numbers between about 10 and 120 certainly do not arise from spallation. With even the most efficient energy transfer mechanism, there is not enough energy available for spallation production of these lower-mass nuclides with the cross sections observed, say at 1 Bev. In looking for other mechanisms one is naturally led to consider fission as a possibility. In a sense the broad and flat yield spectrum in this mass range can be considered to be a culmination of trends already apparent at lower energies. The fission of bismuth with 15–22 Mev deuterons leads to a very narrow fission peak.[27] At 340 Mev this peak has been broadened,[1] and at 480 Mev [2] very small yields of products appear in the valley between the fission and spallation regions and in the light mass region (see Fig. 7). There is also an increasing trend with increasing energy towards greater neutron deficiency of fission products. This latter trend is fairly readily explained in terms of the increasing amount of energy which must be dissipated by particle emission, either before or after fission. Coulomb barrier considerations will favor the evaporation of neutrons with a consequent trend toward neutron deficiency at increasing energies in the medium mass region.

At very low energies, one may probably consider fission as an adiabatic process with the formation of a compound nucleus. Time is available for the excitation energy to distribute itself and reach the specific states for which the fission threshold is lowest. It seems reasonable to suppose that, as the excitation energy goes up the number of accessible states from which fission may occur increases, with a consequent increase in the number of possible fission modes and a decreased specificity of products. Also, up to excitation energies of a few hundred Mev, increased energy deposition presumably leads, by prefission evaporation, to an increasing variety of fissionable nuclides (i.e., nuclides with favorable $Z^2/A$). Both these trends combine to account for the observed broadening of the fission peak up to about 0.5-Bev bombarding energy. Once the evaporation cascade has reached nuclides so far on the neutron-deficient side that proton and neutron evaporation are about equally probable, further increases in excitation energy will not lead to large yields

[24] Currie, Libby, and Wolfgang, Phys. Rev. **101**, 1557 (1956).
[25] F. S. Rowland and R. L. Wolfgang (unpublished data).
[26] Hudis, Baker, and Friedlander, Phys. Rev. **95**, 612 (1954).
[27] A. W. Fairhall, Phys. Rev. **102**, 1335 (1956).

of additional species with favorable $Z^2/A$ ratios. Thus a further increase in the variety of fissionable species is probably not an important factor at bombarding energies above about 0.5 Bev. The flat yield spectrum in the region $40<A<120$ observed at 3 Bev may largely be accounted for by the decreasing specificity of fission modes with increasing excitation of the fissioning nuclei. However, as will be discussed below, another mechanism probably contributes significantly to the yields in this mass range.

The approximate yield-mass curve at 3 Bev (Fig. 7) corresponds to a cross section of about 0.2 barn for production of nuclides in the region $40<A<120$. Since in binary fission two products are formed per nuclear interaction, the fission cross section of lead at 3 Bev is at most about 5% of the total inelastic cross section. As will be discussed below, another mechanism is thought to contribute to the yields in this "fission product" region, and thus the actual fission cross section is probably even smaller. This decrease in the relative abundance of fission processes with increasing bombarding energy above about 0.5 Bev is consistent with the shift of the energy deposition spectrum to higher values. The higher the excitation, the more effectively nucleon evaporation competes with fission, and for sufficiently high initial excitation, the evaporation cascade will continue until the $Z^2/A$ is no longer very favorable for fission. In addition, as will be discussed below, fragmentation is also thought to be a competitive process at high excitation energies.

### 3. *Fragmentation*

With excitation energies of the same magnitude as the total binding energy of the nucleus, it seems unlikely that the nucleus will always retain its spatial integrity long enough for this energy to reach an equilibrium distribution. Furthermore, the proposed energy deposition mechanisms presumably lead to concentration of large amounts of the available energy in relatively small zones of the nucleus. Under such conditions it seems very plausible that fragments of nuclear matter are emitted before anything like equipartition of energy can be established. Fragmentation of this sort would take place in a large variety of modes according to the spatial and momentum distribution of the nucleons participating in the energy-deposition cascade. The rather broad spectrum of fragment sizes (with some favoring of small fragments) which would be expected from such a fast fragmentation mechanism is consistent with the observed yield pattern at Bev bombarding energies. In particular, this mechanism is believed to account for most of the product yields in the range $10<A<40$; but it presumably contributes at larger $A$ values also.

One might think of fragmentation as proceeding by knock-on cascades which break numbers of neighboring nucleon-nucleon bonds and thus produce considerable local disturbances in the nucleus. Surface tension and Coulomb repulsion forces, as well as momentum imparted by the knock-on cascade would tend to separate clumps of still cohering nucleons from each other. These are the progenitors of the final products. With increasing energy and extent of the initial cascade the suggested mechanism would presumably lead to increasing multiplicity and decreasing size of fragments. This trend may be reflected in the fact that the $F^{18}/P^{32}$ and $Na^{24}/P^{32}$ ratios increase by factors of 3 and 5, respectively, as the bombarding energy increases from 0.6 to 3.0 Bev.

The essential characteristic distinguishing the suggested fragmentation mechanism from the more familiar fission process is that it is fast compared to the life of a compound nucleus.[28] The neutron-proton ratios in the initial fragments must then be essentially the same as in the excited nucleus before break-up. Thus light fragments (say $A\sim30$) will initially be very neutron-rich, whereas fragments in the rare-earth region will be near stability. The fragments are in general (although not always) highly excited and may therefore evaporate a sizeable number of nucleons after fragmentation. In the low-mass region the evaporation cascade is expected to tend first towards and then along the stability valley, since Coulomb barriers are low. Maximum yields for each mass number are to be expected along the stability line or slightly to the neutron excess side of it. The high yields of $Na^{24}$ and $P^{32}$ and the somewhat lower ones of $Mg^{28}$ and $P^{33}$ can thus be accounted for. It is felt that the yield of neutron-deficient $F^{18}$ represents only a small fraction of the cross section for producing mass number 18, and that the yield surface actually increases with decreasing $A$ in this region (see Fig. 7). As mentioned earlier, products of still lower $A$ (such as $H^3$, $He^6$, and $Be^7$) are probably largely formed as evaporated particles, although in part their yields may well be due to fragmentation. In fact, there is undoubtedly a continuous gradation, both in product mass

[28] The interpretation of certain high-energy reactions in terms of fragmentation processes grew out of a suggestion by M. L. Perlman and out of discussions in 1953–1954 between R. B. Duffield, G. Friedlander, J. Hudis, J. M. Miller, R. Spence, N. Sugarman, A. Turkevich, and R. Wolfgang. Based on the same discussions, P. Kruger and N. Sugarman, Phys. Rev. **99**, 1459 (1955), used the term and concept of fragmentation to account for some observations on the charge distribution of the products of 450-Mev fission. An essential difference between their interpretation and ours is that they define fragmentation as the emission of light fragments *near stability*. Such a process would require either a redistribution of neutrons and protons during partition, or the emission of the light fragment from a surface layer of approximately equal neutron and proton densities. We prefer to consider the *speed* of the process as the distinguishing characteristic of fragmentation. This would rule out any rearrangement of neutron-to-proton ratios during the process. It appears to us that Kruger and Sugarman's experimental data can be accounted for by fast fragmentation leading to initial excited fragments of equal neutron-to-proton ratio which then evaporate nucleons to reach the observed products; the heavy fragments would have to have rather low excitation energies to account for Kruger and Sugarman's observation of neutron-excess species.

and in time scale, between slow evaporation and fast fragmentation.

The larger entities produced in a fast fragmentation process are also expected to be excited and to emit nucleons. Here, however, the Coulomb barrier favors the emission of neutrons over protons, and the evaporation cascade will tend to cross the stability valley and produce neutron-deficient species. At least part of the yields of the neutron-deficient nuclides between copper and barium may thus be accounted for by fragmentation processes. However, in the medium mass range the present data do not allow a clear-cut distinction between fragmentation and fission, and in the barium region it is not possible to separate the contributions of spallation and fragmentation. However, if fragmentation reactions account for the formation of the light products ($A<35$), there could be partners of these fragments in the region of $A\sim120$ to 160, and some of the observed barium yields may thus well be due to this mechanism. Preliminary data on recoil ranges of barium isotopes[7,12] and sodium-24[29] from bismuth are consistent with this picture, although the recoil behavior of the barium isotopes can be accounted for equally well by a spallation mechanism.[12]

## ACKNOWLEDGMENTS

The authors are greatly indebted to Professor R. B. Duffield, Professor J. M. Miller, Dr. M. L. Perlman, Professor N. Sugarman, Professor A. Turkevich and Professor V. F. Weisskopf for helpful and stimulating discussions. The performance of numerous chemical yield analyses by Dr. R. Stoenner, Dr. K. Rowley, and Miss E. Norton, and the assistance of Mrs. J. Eliot, Miss G. Vedder, and Mrs. N. Hamilton with the radioactivity measurements are gratefully acknowledged. It is a pleasure to thank the operating staffs of the Cosmotron and of the Nevis cyclotron for their cooperation.

## APPENDIX

In this appendix all the chemical procedures used and the counting efficiencies assumed for those nuclides not decaying by 100% hard beta emission are discussed briefly. Except where otherwise noted the chemical separations were initiated by dissolving the irradiated lead foils in $6N$ $HNO_3$ containing 2–10 mg amounts of each of the appropriate carriers. In general, the procedures then followed are modifications of those given by the Los Alamos[30] and Berkeley groups.[31] Most of the data for the calculation of the counting efficiencies were taken from the compilations of Hollander, Perlman, and Seaborg[32] and Way *et al.*[33]

### Fluorine

The $HNO_3$ solution of the target was buffered with ammonium acetate and the fluorine precipitated with HCl as PbClF. $HClO_4$ was added to this precipitate and $H_2SiF_6$ was steam distilled into acetate-buffered $PbCl_2$ solution. The steam distillation was repeated and the $H_2SiF_6$ caught in acetate-buffered $Ca(NO_3)_2$. The $CaF_2$ obtained was mounted.

### Sodium

Sodium was separated from a $HNO_3$ solution from which a number of elements had already been removed. Any remaining Pb was precipitated out as $PbCl_2$. The decontamination procedure followed was essentially that of reference 30 (page 29) with the additional step of removing $K^+$ as $KClO_4$ just prior to the final precipitation of NaCl.

### Magnesium

Magnesium was usually isolated after removal of phosphorus as zirconium phosphate. A sulfide precipitation of any Cd, Mo, and Pb was followed by two or three $Fe(OH)_3$ scavenging precipitations. The last supernate was evaporated, taken up in $9N$ HCl, and passed through a Dowex 1 column. Scavenge precipitations of CuS in $0.3N$ HCl and of $Fe(OH)_3$ were made. Evaporation to dryness, removal of $NH_4$ salts by fuming, and precipitation of $MgCO_3$ with $(NH_4)_2CO_3$ and ethyl alcohol followed. The $MgCO_3$ was dissolved in HCl, and two or three precipitations of Ba and Sr carriers with fuming $HNO_3$ or with $CrO_4^=$ were carried out and followed by a $CaC_2O_4$ precipitation. Finally the magnesium was precipitated and mounted as $MgNH_4PO_4$.

Because the product of the $Mg^{28}$ beta decay is the 2.3-min beta emitting $Al^{28}$, a counting efficiency of 2.0 was assumed.

### Phosphorus

Zirconium phosphate was isolated from the target solution by the addition of $ZrO^{++}$. This precipitate was dissolved in HF and ammonium phosphomolybdate precipitated. This was dissolved in $NH_3$, a few drops $H_2O_2$ were added and zirconium phosphate was reprecipitated in $6N$ HCl. HF was added and $As_2S_3$ and $LaF_3$ scavengings in $3N$ HCl were made. Ammonium phosphomolybdate was reprecipitated and dissolved in $NH_3$. $V^{+3}$ and excess citric acid were added and $SO_2$ passed in. The phosphorus was finally precipitated and mounted as $MgNH_4PO_4$.

Due to the difficulty of decay curve analysis the cross sections reported for $P^{33}$ are expected to be accurate only to $\pm50\%$.

### Manganese

Mn was separated from the supernate after the initial PbClF precipitation in the fluoring procedure. To avoid difficulties resulting from possible slow exchange between Mn oxidation states, the Mn II was oxidized to Mn VII with $NaBiO_3$ and reduced back to Mn II with $H_2O_2$. $MnO_2$ was precipitated by addition of $16N$ $HNO_3$ and $KClO_3$. This precipitate was dissolved in $H_2O_2$ and $6N$ $HNO_3$, holdback carriers of elements with soluble hydroxides were added, and $MnO_2$ was reprecipitated with $Na_2O_2$. The $MnO_2$ was dissolved in fuming $HNO_3$ and Ti IV and Ta IV were added and precipitated by boiling. The cycle of alternating precipitations of $MnO_2$ by $KClO_3$ and $Na_2O_2$ was repeated three times. The $Mn^{++}$ resulting was oxidized to $MnO_4^-$ and an $Fe(OH)_3$ scavenging precipitation was made. The $MnO_4^-$ was reduced with $H_2C_2O_4$ and an acid sulfide scavenging precipitation of Sb, Sn, and Te carried out. $MnO_2$ was again precipitated with acid $KClO_3$ and mounted.

### Iron

The $Fe(OH)_3$ obtained from the ether extraction (as described in the Mo procedure) was decontaminated by the procedure given

[29] J. Hudis (unpublished results).
[30] J. Kleinberg *et al.*, U. S. Atomic Energy Commission Report LA 1566, February 1, 1953 (unpublished).
[31] W. W. Meinke, U. S. Atomic Energy Commission Report AECD 2738, 1949 (unpublished).
[32] Hollander, Perlman, and Seaborg, Revs. Modern Phys. **25**, 469 (1953).
[33] Way, Fuller, Hankins, King, Kundu, McGinnis, van Lieshout, and Wood, Nuclear Sci. Abstracts **7**, No. 24B (1953); **8**, No. 24B (1954); and **9**, No. 24B (1955).

in reference 30 (page 59). The final precipitate mounted was $Fe(OH)_3$. The counting efficiency of $Fe^{59}$ was taken as unity and that of $Fe^{52}$ as 1.4.

## Copper

After removal of Ba, Sr, Pb, and Mn the $HNO_3$ solution was evaporated to dryness. The residue was taken up in 1*N* HCl, CuS precipitated and then dissolved in $HNO_3$. The scavenging precipitations of $Fe(OH)_3$ and $BaCO_3$ from $NH_3$ solution were then carried out. CuS was precipitated from 1*N* HCl and redissolved. The solution was made barely ammoniacal and scavenged twice with CdS in the presence of KCN. After boiling out the HCN, CuCNS was precipitated from 0.5*N* HCl by addition of $NaHSO_3$ and KCNS. The precipitate was dissolved in $HNO_3$ and CuCNS reprecipitated. This was redissolved and two AgCl scavengings were made. The Cu was finally precipitated and mounted as CuCNS.

To correct for electron capture branching, counting efficiencies of 0.71 for $Cu^{61}$ and 0.60 for $Cu^{64}$ were used. Owing to the difficulty in decay curve analysis arising from the low yield of $Cu^{61}$, cross sections reported for this nuclide have an estimated error of $\pm 50\%$.

## Zinc

Zinc was precipitated as the alkaline sulfide from the supernate of the first CuS precipitation in the copper procedure. The initial decontamination procedure was that given in reference 31 (page 77, steps 1–5). The residue from the HBr evaporation was taken up in 2*N* HCl and run through a Dowex-1 column. After washing with additional 2*N* HCl the Zn was eluted with 1*N* $NH_3$ and precipitated for mounting as ZnS.

A counting efficiency of 2.5 was used for the $Zn^{72}$ in equilibrium with $Ga^{72}$. Owing to difficulty in decay curve analysis, an uncertainty of about $\pm 50\%$ is assigned to the cross section of $Zn^{71m}$. The cross section values given for $Zn^{62}$ were obtained by chemically separating $Cu^{62}$ from a previously separated zinc sample.

## Gallium

Gallium was separated from the supernate following precipitation of Mo with $\alpha$-benzoin oxime (see Mo procedure). The solution was evaporated with $HNO_3$ and taken up in 8*N* HCl. The Ga was extracted into isopropyl ether, back extracted into water and precipitated as the ferrocyanide. The precipitate was digested with $HNO_3$ and taken up in 8*N* HCl containing Fe, Au, Tl carriers. $SnCl_2$ was added and the Ga was extracted into isopropyl ether and back extracted into water. $Fe^{+3}$ was added and precipitated with NaOH. The Ga was finally precipitated as the 8-hydroxy quinolate at $p$H$\sim$6.

The absolute disintegration rate of $Ga^{67}$ was determined using a cross-calibration of the counter used with an x-ray counter of known geometry. Because of poor checks in duplicate runs, the $Ga^{67}$ results are thought to be accurate to only a factor of 2 and the $Ga^{72}$ results within $\pm 40\%$.

## Molybdenum

HCl was added to the supernate of the zirconium phosphate precipitation (see phosphorus procedure) and $PbCl_2$ removed. The supernate was evaporated, taken up in 6*N* HCl containing $Br_2$, and extracted with ethyl ether. Water was added to the ether phase, the ether was evaporated, and the Fe present was precipitated as $Fe(OH)_3$ with NaOH. Mo was precipitated by addition of $HNO_3$, oxalic acid, and $\alpha$-benzoin oxime. The organo-molybdenum compound was destroyed with $HClO_4$, $NH_3$ was added, and $Fe(OH)_3$ was precipitated. The supernate was acidified with $H_2SO_4$ and the final $Ag_2MoO_4$ precipitation was carried out in acetate buffer.

The counting efficiency of the isomeric transition of $Mo^{93m}$ was taken to be 0.9 in accordance with the findings of Kundu *et al.*[34]

## Cadmium

Cadmium was isolated from the aqueous phase remaining after ether extraction of Mo, Fe, and Ga (see Mo procedure). The Cd in this solution was decontaminated by the procedure given in reference 31 (p. 138). The final precipitate mounted and counted was CdS.

The counting efficiency of $Cd^{115m}$ is 1.0. From the published decay data the efficiency of the $Cd^{115}$ in equilibrium with its $In^{115m}$ daughter was calculated to be 1.29. $Cd^{107}$ was counted through the 94-kev conversion electrons of its daughter $Ag^{107m}$. The counting efficiency of 0.75 assumed for this radiation is approximate and an error of $\pm 40\%$ is estimated for the cross sections given. $Cd^{117m}$ in equilibrium with its daughters was taken to have a counting efficiency of 2. An error of $\pm 50\%$ is assigned to these cross sections because of uncertainties arising from analysis of the complex decay curves.

## Barium

Barium was decontaminated and separated by the procedure given in reference 31 (p. 173).

The counting efficiency of the $Ba^{128}$ in equilibrium with $Cs^{128}$ was taken to be 1.0. $Ba^{131}$ was couuted on a scintillation counter. The product of the counting efficiency of $Ba^{131}$ and of the geometry of the counter used was calculated using $\gamma$ and x-ray calibrations at various energies. The counting efficiency of $Ba^{140}$ was taken as $\sim$2 and that of $Ba^{133m}$ and $Ba^{135m}$ as $\sim$0.7.

[34] Kundu, Hult, and Pool, Phys. Rev. **77**, 71 (1950).